1238 *Biochemistry* **2011,** *50,* 1238–1246
DOI: 10.1021/bi101774g

BIOCHEMISTRY
including biophysical chemistry & molecular biology
Article

Molecular Investigations of the Structure and Function of the Protein Phosphatase 1−Spinophilin−Inhibitor 2 Heterotrimeric Complex[†]

Barbara Dancheck,[‡,#] Michael J. Ragusa,[§,#] Marc Allaire,[∥] Angus C. Nairn,[⊥] Rebecca Page,[§] and Wolfgang Peti*[,‡]

[‡]*Department of Molecular Pharmacology, Physiology and Biotechnology, and* [§]*Department of Molecular Biology, Cell Biology, and Biochemistry, Brown University, Providence, Rhode Island 02912, United States,* [∥]*National Synchrotron Light Source, Brookhaven National Laboratory, Upton, New York 11973, United States, and* [⊥]*Department of Psychiatry, Yale University School of Medicine, New Haven, Connecticut 06511, United States.* [#]*These authors contributed equally to this work*

Received November 4, 2010; Revised Manuscript Received January 6, 2011

ABSTRACT: Regulation of the major Ser/Thr phosphatase protein phosphatase 1 (PP1) is controlled by a diverse array of targeting and inhibitor proteins. Though many PP1 regulatory proteins share at least one PP1 binding motif, usually the RVxF motif, it was recently discovered that certain pairs of targeting and inhibitor proteins bind PP1 simultaneously to form PP1 heterotrimeric complexes. To date, structural information for these heterotrimeric complexes and, in turn, how they direct PP1 activity is entirely lacking. Using a combination of NMR spectroscopy, biochemistry, and small-angle X-ray scattering (SAXS), we show that major structural rearrangements in both spinophilin (targeting) and inhibitor 2 (I-2, inhibitor) are essential for the formation of the heterotrimeric PP1−spinophilin−I-2 (PSI) complex. The RVxF motif of I-2 is released from PP1 during the formation of PSI, making the less prevalent SILK motif of I-2 essential for complex stability. The release of the I-2 RVxF motif allows for enhanced flexibility of both I-2 and spinophilin in the heterotrimeric complex. In addition, we used inductively coupled plasma atomic emission spectroscopy to show that PP1 contains two metals in both heterodimeric complexes (PP1−spinophilin and PP1−I-2) and PSI, demonstrating that PSI retains the biochemical characteristics of the PP1−I-2 holoenzyme. Finally, we combined the NMR and biochemical data with SAXS and molecular dynamics simulations to generate a structural model of the full heterotrimeric PSI complex. Collectively, these data reveal the molecular events that enable PP1 heterotrimeric complexes to exploit both the targeting and inhibitory features of the PP1-regulatory proteins to form multifunctional PP1 holoenzymes.

PP1[1] is a major Ser/Thr protein phosphatase with roles in numerous cellular processes including cell cycle progression, protein synthesis, muscle contraction, transcription, and neuronal signaling (*1*, *2*). Two metals in the active site of PP1 mediate a single step dephosphorylation reaction. The metal ions enhance the nucleophilicity of a water molecule bound at the active site, which performs nucleophilic substitution with the phosphate moiety (*3*, *4*). *In vitro* these metals are often manganese, as PP1 is expressed in the presence of manganese. *In vivo* it is believed that these metal ions are iron and zinc (*4*). The surface of PP1 is characterized by extensive grooves, including three potential substrate interaction sites: the acidic, the hydrophobic, and the C-terminal substrate binding grooves. Due to its large number of functions, PP1 is active toward a broad range of substrates (*5*). Despite this inherent lack of substrate specificity, dephosphorylation events by PP1 are under exceedingly tight control. This strict regulation of PP1 activity is mediated by a large number of diverse regulatory proteins (∼200) (*5*, *6*). There are two types of regulatory proteins: 1) targeting proteins that direct PP1 to specific locations in the cell and alter its substrate specificity and 2) inhibitor proteins (*7*, *8*). Notably, these regulatory proteins have very little sequence similarity. In addition, structures of PP1 in complex with the targeting proteins spinophilin/neurabin (*9*) and MYPT1 (*10*) and the inhibitor protein inhibitor 2 (I-2) (*11*, *12*) demonstrate the diversity of regulatory protein interactions with PP1. From these structures it has become evident that targeting proteins regulate PP1 by differentially altering its ability to bind substrates. Spinophilin blocks the C-terminal groove (*9*), while MYPT-1 appears to extend the acidic groove of PP1 (*10*). Recently, it was shown that specific pairs of targeting and inhibitor proteins can bind PP1 simultaneously, adding an additional layer of complexity to PP1 regulation (*13*−*15*). Despite the recent advances in structural information for heterodimeric complexes of PP1, structural information for heterotrimeric PP1 complexes is entirely missing.

One heterotrimeric PP1 complex of interest is PP1−spinophilin−I-2 (PSI). Spinophilin is a multidomain scaffolding protein which targets PP1 to dendritic spines and is important for the regulation

[†]This material is based upon work supported by a National Science Foundation Graduate Research Fellowship to B.D. The project described was supported by Grant R01NS056128 from the National Institute of Neurological Disorders and Stroke to W.P. and an American Cancer Society research scholar grant (RSG-08-067-01-LIB) to R. P. 800 MHz NMR data were recorded at Brandeis University (NIH S10-RR017269). Use of the National Synchrotron Light Source, Brookhaven National Laboratory, was supported by the U.S. Department of Energy, Office of Science, Office of Basic Energy Sciences, under Contract No. DE-AC02-98CH10886.

*Corresponding author. Phone: 401-863-6084. Fax: 401-863-6087. E-mail: Wolfgang_Peti@brown.edu.

[1]Abbreviations: NMR, nuclear magnetic resonance; SAXS, small angle X-ray scattering; ICP-AES, inductively coupled plasma atomic emission spectroscopy; PP1, protein phosphatase 1; I-2, inhibitor 2; PI, PP1−inhibitor 2 complex; PS, PP1−spinophilin complex; PSI, PP1−spinophilin−I-2 complex.

 Published on Web 01/10/2011

of excitatory synaptic transmission and synaptic plasticity (*16*−*18*). I-2 is a ubiquitous, single domain inhibitor of PP1 found in diverse tissues such as brain, skeletal muscle, and sperm (*19*). As cells progress to the S phase of the cell cycle (*20*), I-2 is translocated into the nucleus and its expression peaks during S-phase and mitosis (*21*), indicating a role for I-2 in cell cycle regulation. *In vitro*, I-2 forms an inactive complex with PP1 that can be reactivated by phosphorylation of I-2 at Thr72 by glycogen synthase kinase 3 or cyclin-dependent kinase 2. Recently, spinophilin (or its neuronal isoform neurabin) and I-2 were shown to bind PP1 simultaneously to form a heterotrimeric complex (PSI). Furthermore, I-2 and neurabin were shown to colocalize in actin-rich adherens junctions and dendritic spines (*13*), suggesting a role for the heterotrimeric PSI complex in cytoskeletal rearrangement and/or neuronal signaling. Once targeted to the dendritic spine and cytoskeleton, the PSI complex is poised for immediate activation from signaling pathways which may lead to the phosphorylation of I-2 and reactivation of the phosphatase.

Most PP1 regulatory proteins bind PP1 via a common docking motif termed the RVxF motif. This short consensus motif binds PP1 in a hydrophobic pocket ~20 Å from the active site. The necessity of this interaction site for interaction with PP1 is the reason that it was originally thought that only one regulatory protein could bind PP1 at a time. This view has changed over the last ten years, with the identification of the PSI complex, as well as the identification of three additional heterotrimeric PP1 complexes, including the PP1−GADD34−I-1, the PP1−Sds22−I-3 and the PP1−MYPT1−CPI-17 complexes (*14*, *15*, *22*). However, GADD34 and I-1 also interact in the absence of PP1. Moreover, CPI-17 does not contain an RVxF motif; rather it is a highly specific inhibitor of the PP1−MYPT1 holoenzyme. Lastly, Sds22 also does not contain an RVxF motif. Thus, only in the PSI complex do both PP1 regulators, spinophilin and I-2, contain a RVxF motif and require PP1 for the formation of the heterotrimeric complex (*13*).

The PP1−spinophilin (PS) and PP1−I-2 (PI) complex structures have been solved by X-ray crystallography and NMR spectroscopy-based ensemble calculations (*9*, *11*, *12*). These structures provide insights into the mechanisms each protein uses to regulate PP1. While both proteins form unique interactions with PP1, they also share common binding sites. First, both spinophilin and I-2 bind PP1 via the RVxF motif (*9*, *11*, *23*). Second, helices from I-2 and spinophilin bind in a similar location on PP1 near the hydrophobic groove, with residues Asp163 of I-2 and Glu482 and Glu486 of spinophilin making contacts with Arg132 of PP1. Therefore, a structural rearrangement of I-2, spinophilin, or both proteins is necessary for the formation of the heterotrimeric PSI complex. We have used NMR spectroscopy, biochemistry, and small angle X-ray scattering (SAXS) to gain insight into the formation and regulation of PSI. In combination with the previously reported structures of the heterodimeric complexes, our data provide the first structural insights into a heterotrimeric PP1 complex and provide a model for how these complexes direct PP1 activity *in vivo*.

MATERIALS AND METHODS

Protein Expression and Purification. Unlabeled PP1α_{7-330}, unlabeled spinophilin$_{417-583}$, and both unlabeled and $^{2}H,^{15}N$-labeled I-2_{9-164}C85S were produced as previously described (*9*, *12*, *24*, *25*). As NMR spectroscopy becomes increasingly more difficult with increasing size of proteins, the shortest, but fully biologically active constructs of spinophilin and I-2 were used for all NMR experiments. Both constructs contain the total binding activity for PP1. The spinophilin construct included the neighboring PDZ domain to enhance stability of spinophilin in solution. The C85S mutation of I-2 was used because wild-type I-2 dimerizes by forming an artificial disulfide bond (dimer formation can be reversed by reducing agents), and this dimerization is not observed with I-2C85S. The expression of $^{2}H,^{15}N$-labeled spinophilin$_{417-583}$ was carried out by growing freshly transformed BL21-Codon-Plus (DE3)-RIL cells (Stratagene) in M9 minimal medium containing 1 g/L $^{15}NH_4Cl$ as the sole nitrogen source, prepared in D_2O. Protein expression was induced with 1 mM IPTG. $^{2}H,^{15}N$-labeled spinophilin$_{417-583}$ was purified following the same protocol as unlabeled spinophilin$_{417-583}$. The PS and PI complexes were produced as previously described (*9*, *12*) with the following minor modifications. After elution from the Ni-NTA column, the complexes were purified using a Superdex 200 26/60 size exclusion column (GE Healthcare) equilibrated with PP1 complex buffer (20 mM Tris, pH 7.5, 50 mM NaCl, 0.5 mM TCEP). Tobacco etch virus protease was added to cleave the His_6-tag from PP1α_{7-330}. After digestion was complete, the complexes were loaded onto Ni-NTA beads, from which they eluted in the flow-through. For the final purification step, the proteins were purified using a Superdex 75 26/60 size exclusion column (GE Healthcare) equilibrated with PP1 complex buffer.

For the production of the PSI complex, PP1α_{7-330} was bound to Ni-NTA beads via its His_6-tag and incubated with purified, untagged spinophilin$_{417-583}$. Following step elution with buffer containing 250 mM imidazole, the eluate was loaded directly onto a Superdex 200 26/60 size exclusion column equilibrated with PP1 complex buffer. Fractions containing the PS complex were confirmed by SDS−PAGE gel electrophoresis. The complex was pooled, and TEV protease was added to remove the His_6 tag from PP1 overnight. After digestion was complete, the complex was incubated with a 1:2 molar ratio of >98% pure I-2_{9-164}, and the complex was loaded onto a Superdex 75 26/60 size exclusion column equilibrated with PP1 complex buffer. The heterotrimeric PSI complex eluted from this column at ~127 mL. Fractions containing the PSI complex were confirmed by SDS−PAGE gel electrophoresis.

The QuikChange site-directed mutagenesis kit (Stratagene) was used to create the C85S, I13A/L14A/K15A, K42A/Q44G, W46A, and R157A/D163A mutants of I-2 following the manufacturer's protocol. The presence of the mutations was confirmed by sequencing. All mutants were prepared following the same protocol as I-2_{9-164}C85S. CD spectroscopy was used to confirm that mutagenesis of I-2 did not alter the overall secondary structure of the protein. CD spectra and estimation of percent α-helical content of the I-2 mutants were performed as previously reported (*25*).

NMR Spectroscopy. Samples for NMR spectroscopy were prepared in 20 mM Tris, pH 7.5, 50 mM NaCl, and 0.5 mM TCEP. The 2D $[^{1}H,^{15}N]$-HSQC spectra of unbound I-2 and unbound spinophilin were measured at 298 K on a Bruker Avance II 500 MHz spectrometer equipped with a TCI HCN *z*-gradient cryoprobe. The 2D $[^{1}H,^{15}N]$-TROSY spectra of the PS, PI, and PSI complexes were measured at 298 K on a Bruker Avance II 800 MHz spectrometer equipped with a TCI HCN *z*-gradient cryoprobe. The NMR spectra were processed with Topspin 1.3 (Bruker) and analyzed with the CARA software package (www.nmr.ch). Chemical shift differences ($\Delta\delta$) were calculated as $\Delta\delta$ (ppm) = $[(\Delta\delta_H)^2 + (\Delta\delta_N/10)^2]^{1/2}$.

Inductively Coupled Plasma Atomic Emission Spectroscopy. The manganese content of the PS, PI, and PSI complexes was measured using a Jobin Yvon JY2000 inductively coupled plasma atomic emission spectrometer. Complexes were prepared as described, concentrated, and then diluted in 2% nitric acid. Manganese standards were prepared in 2% nitric acid. Three independent measurements were performed in triplicate for each sample.

pNPP Assay. Dephosphorylation of *p*NPP by P, PI, and PSI was carried out by the incubation of PP1 alone or the PI or PSI complexes with 0.5, 1, 2, 4, and 8 mM pNPP. Reactions were incubated for 30 min at 30 °C and were quenched by addition of 1 M NaOH. The amount of *p*-nitrophenolate product was determined from the absorbance at 405 nm using a molar extinction coefficient of 18000 M^{-1} cm^{-1}. Sigmaplot (Systat Software Inc.) was used to determine the K_M and k_{cat} for each complex against pNPP.

Capture Assay. For the capture assay using PP1, cells expressing His_6-tagged PP1α_{7-330} were lysed by high-pressure homogenization (Avestin C-3 Emulsiflex). His_6-tagged PP1α_{7-330} was bound to Ni-NTA beads (Qiagen, six parallel 1 mL columns with fresh beads). For the capture assay using the PS complex, PS was prepared as described above up until the TEV cleavage step. The PS complex was bound to Ni-NTA beads via the His_6-tag on PP1α_{7-330} (Qiagen, six parallel 1 mL columns with fresh beads). The beads were extensively washed and subsequently incubated with buffer, I-2_{9-164}C85S, or one of the four I-2 mutants for 1 h at 4 °C. After extensive washing to remove any unbound I-2, the PI or PSI complexes were eluted with elution buffer containing 1 M imidazole. Bound complexes were analyzed by SDS−PAGE using Coomassie blue staining, and the density of the protein bands was quantified using the Quantity One program (Bio-Rad Laboratories).

Small Angle X-ray Scattering. Small angle X-ray scattering (SAXS) data were recorded on the PSI complex. Samples were prepared in 20 mM Tris, pH 7.5, 50 mM NaCl, and 0.5 mM TCEP within 24 h of data acquisition and were stored at 4 °C. Prior to scattering experiments the samples were concentrated and filtered through a 0.02 μm filter (Whatman). Scattering data were collected at the National Synchrotron Light Source (NSLS) beamline X9 using a MarCCD 165 located at 3.4 m distance from the sample for small angle X-ray data. Wide angle X-ray scattering (WAXS) data were collected simultaneously with SAXS data using a Photonic Science CCD located at 0.47 m from the sample. Twenty microliters of sample was continuously flowed through a 1 mm diameter capillary and exposed to a 400 × 200 μm X-ray beam for 180 s of total measurement time. Scattering data for the PSI complex were collected at 0.8 and 1.2 mg/mL. PRIMUS was used for normalization of changes in the beam intensity, buffer subtraction, and merging of the small angle and wide angle scattering data (*26*). The radius of gyration (R_g) was calculated using a Guinier approximation, $I(q) = I(0)\exp(-q^2R_g^{2/3})$, where a plot of $I(q)$ and q^2 is linear for $q < 1.3/R_g$ (*27*). Four independent scattering trials were averaged. The linearity of the Guinier plots was evaluated to confirm that no aggregation was present in any of the samples. HYDROPRO was used to calculate the R_g for the PSI model (*28*). GNOM was used to determine the pair distribution function [$P(r)$] and maximum particle dimension (Dmax) (*29*). Sixteen independent *ab initio* models were calculated using GASBOR (*30*). The models were aligned and averaged using DAMAVER (*31*). The averaged *ab initio* envelope was aligned with the PSI model using SUPCOMB (*32*). BILBOMD was used to investigate the flexibility of the PSI complex (*33*). Molecular dynamics (MD) simulations as part of BILBOMD were used to generate 12000 structures with a R_g range of 20−50 Å (200 structures/1 Å; two total calculations). Theoretical scattering curves were calculated for each structure using FOXS and compared to the experimental data (*34*). The single best fit structure is defined as the structure with the lowest discrepancy (χ^2) between the theoretical and experimental data. A minimal ensemble (MES) model was generated as previously described; this is the minimal number of either two, three, four, or five structures that provided the smallest discrepancy between theoretical and experimental scattering data (*33*). This ensemble was selected as the best model for the protein complex in solution.

RESULTS

Spinophilin$_{417-583}$, I-2_{9-164}C85S, and PP1α_{7-330} Form a Stable Heterotrimeric Complex in Vitro. Size exclusion chromatography (SEC) was used to determine whether spinophilin$_{417-583}$, I-2_{9-164}C85S, and PP1α_{7-330} form a stable heterotrimeric complex *in vitro*. Briefly, the PS complex was incubated with a 1:2 molar ratio of I-2_{9-164}, and the formed complex was injected onto a Superdex 75 26/60 size exclusion column. The heterotrimeric PSI complex eluted at ∼127 mL, prior to excess unbound I-2 (Figure 1). For comparison, both PS and PI elute at ∼155 mL, demonstrating a significant increase in molecular size upon formation of the heterotrimeric PSI complex. SDS−PAGE gel electrophoresis confirmed the presence of all three proteins in the appropriate stoichiometric ratios (Figure 1). Additionally, we have measured the activity of P, PI, and PSI against pNPP, a commonly used substrate in phosphatase assays (Supporting Information Table S1). The K_M of PP1, PI, and PSI for pNPP is 2.5 ± 0.7, 6.9 ± 0.2, and 6.7 ± 0.2 mM, respectively. These data demonstrate that I-2 is active as a competitive inhibitor of PP1 in both the PI and PSI complexes. Taken together, these data demonstrate the stable formation of the heterotrimeric PSI complex *in vitro*.

Two Manganese Ions Are Present in the Active Site of All Three PP1 Complexes. Two manganese ions are present in the active site of PP1 in the crystal structure of the PS complex (*9*) and the PP1−MYPT1 complex (*10*). In contrast, only one manganese ion was observed in the crystal structure of the PI complex (*11*), suggesting that I-2 may expel one of the metals from the active site of PP1 as a mechanism of inhibition. To determine the number of Mn^{2+} ions in the heterodimeric PS, the heterodimeric PI, and the heterotrimeric PSI complex in solution, we used inductively coupled plasma atomic emission spectroscopy (ICP-AES). The results are summarized in Table 1. As expected, 2 mol of manganese was present per mole of PS. In addition, 2 mol of manganese was also present per mole of both PI and PSI. Thus, these data show that PSI retains the biochemical characteristics of the PS and PI holoenzymes.

The I-2 RVxF Motif Is Not Necessary for Stable PP1 Binding. An overlay of the crystal structures of the PS and PI complexes reveals two regions of steric clashing between I-2 and spinophilin (Supporting Information Figure S1). Thus, to form the heterotrimeric PSI complex, either spinophilin, I-2, or both must undergo a conformational rearrangement. In order to understand the structural rearrangements that occur during the formation of PSI, we undertook NMR spectroscopy studies of PS (55.9 kDa), PI (55.2 kDa), and PSI (73.9 kDa). For these studies, only a single protein (either I-2 or spinophilin) was ^2H,^{15}N isotopically labeled and, thus, NMR active; the other proteins of the heterotrimeric

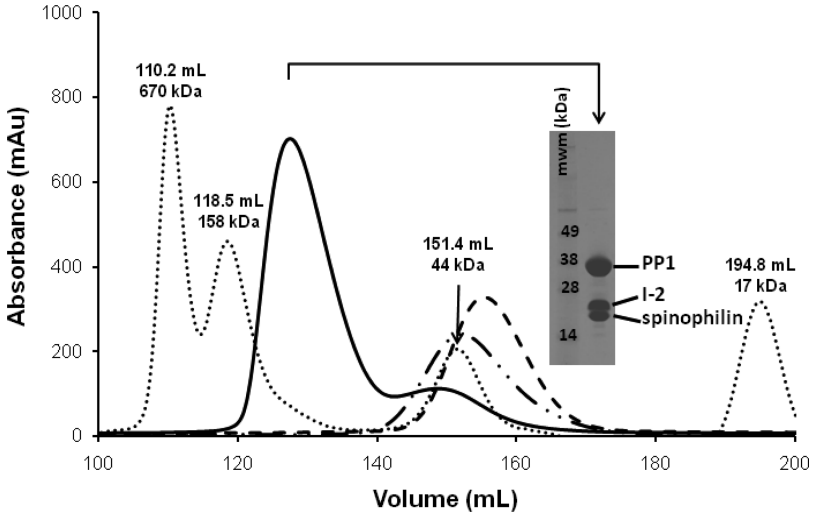

FIGURE 1: PP1, spinophilin, and I-2 form a stable, heterotrimeric complex. Superdex 75 26/60 SEC chromatograms are shown for PS (dashed line), PI (dashed-dotted line), PSI (solid line), and a series of molecular mass standards (dotted line). In the PSI chromatogram, distinct peaks are observed for the PSI complex at 127 mL and for excess, unbound I-2 at 149 mL (void volume ~100 mL). The PSI chromatogram is overlaid with that of PS and PI alone, illustrating the shift in elution position upon complex formation. The SDS−PAGE gel to the right of the chromatogram shows that I-2 and spinophilin are bound to PP1 in a 1:1 stoichiometric ratio and that the complex is highly pure.

Table 1: Manganese Content of PS, PI, and PSI Complexes As Measured by ICP-AES[a]

complex	mol of Mn^{2+}/mol of complex	standard deviation
PS	2.3	0.3
PI	1.9	0.1
PSI	2.4	0.3

[a]Values are the average of three independent measurements performed in triplicate.

complex remained unlabeled, and, thus, invisible in the NMR spectra. This makes the analysis of the NMR spectra much more feasible for these high molecular mass complexes (> 55 kDa).

We previously completed the sequence-specific backbone assignment of I-2 in both the unbound and PP1-bound states (*12*, *25*). We subsequently demonstrated that regions of I-2 with significant chemical shift differences between unbound I-2 and PP1-bound I-2 were limited to the three regions that directly interact with PP1, specifically the RVxF motif, the SILK motif, and the C-terminal helix (*12*). The SILK motif is a previously identified interaction site of I-2 with PP1 (*6*, *35*, *36*). These experiments confirmed that large regions of I-2, including residues 55−127, remain flexible in the PP1-bound state. Figure 2A depicts an overlay of the 2D [^{1}H,^{15}N]-HSQC spectrum of unbound ^{15}N-labeled I-2 and the 2D [^{1}H,^{15}N]-TROSY spectrum of ^{2}H,^{15}N-labeled I-2 in PSI while Figure 2B depicts an overlay of the 2D [^{1}H,^{15}N]-TROSY spectra of ^{2}H,^{15}N-labeled I-2 in the PI and PSI complexes. The spectra in Figure 2B are highly similar, indicating that no major structural rearrangement of I-2 between the PI and PSI complexes occurs. The differences in the spectra are quantified using chemical shift difference plots, which are shown in Figure 2C (unbound I-2 versus I-2 in PSI) and Figure 2D (I-2 in PI versus I-2 in PSI). The regions of I-2 with significant chemical shift differences between unbound I-2 and PSI are the SILK motif, which binds the back side of PP1, and the C-terminal helix, which lies over the PP1 active site. In contrast, there are essentially no differences in the RVxF motif between unbound I-2 and PSI. This shows that the RVxF motif is not bound to PP1 in the PSI complex. This is further supported by that observation that the RVxF motif is the only region of I-2 with significant chemical shift differences when comparing the chemical shifts of I-2 in PI and PSI complexes.

Pull Downs of I-2 Mutants Identify the SILK Motif as Critical for PSI Formation. To complement the NMR analysis of each of the three PP1-binding motifs of I-2 in the formation of the PI versus PSI complexes, numerous I-2 point mutants were created and used in pull-down assays to test their ability to form the PSI complex. I-2C85S was used as the wild-type control (*11*). The SILK mutant, I13A/L14A/K15A, includes residues forming both electrostatic and hydrophobic interactions with PP1. The RVxF (residues $KSQKW^{42-46}$ in I-2) mutant 1, W46A, was created because W46 is buried in a hydrophobic pocket in the RVxF motif binding groove and plays an essential role in forming the PI complex. However, we have previously shown that W46 is also important in the stabilization of transient tertiary structure in unbound I-2 (*12*, *25*). In order to confirm that our results were not due to a destruction of important tertiary structure in unbound I-2, an additional RVxF mutant 2, K42A/Q44G, was produced; these residues also make important contacts with PP1. Finally, the C-terminal helix mutant, R157A/D163A, was created because these residues form important electrostatic interactions with PP1 in the PI complex. CD spectroscopy confirmed that mutagenesis did not alter the secondary structure present in unbound I-2 (Supporting Information Figure S2).

As shown in Figure 2E, all three PP1 binding motifs of I-2 are equally important in the formation of the PI complex, as all mutations affected the binding of I-2 to PP1 alone about equally (~20−40% reduction in binding; black bars). In contrast, the SILK motif mutant, in agreement with our NMR data, resulted in significantly less binding of I-2 to the PS complex (~85% reduction in binding) when compared with all other I-2 mutants (gray bars). Therefore, upon release of the I-2 RVxF motif from PP1, the SILK motif becomes critically important for I-2 to bind PS and form the heterotrimeric PSI complex.

Collectively, these data show that the RVxF motif of I-2 is in a similar environment in unbound I-2 and PSI, i.e., not bound to PP1, while the SILK motif and C-terminal helix are in similar environments in the PI and PSI complexes, i.e., bound to PP1.

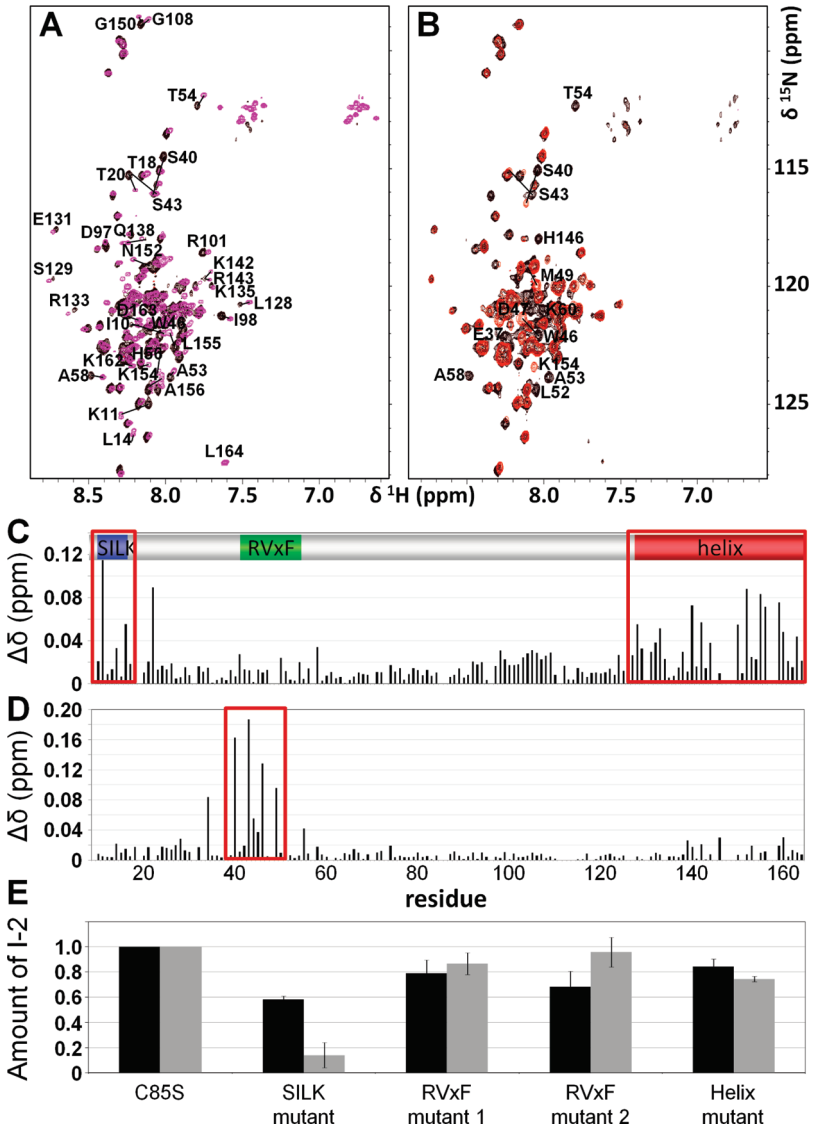

FIGURE 2: The RVxF motif of I-2 is released from PP1 in the formation of PSI, increasing the importance of the SILK motif. (A) Overlay of the [^{1}H,^{15}N]-HSQC spectrum of unbound I-2 (pink) and the [^{1}H,^{15}N]-TROSY spectrum of PSI-bound I-2 (black). Peaks undergoing chemical shift changes are annotated. (B) Overlay of the [^{1}H,^{15}N]-TROSY spectra of PSI-bound I-2 (black) and PI-bound I-2 (red). (C) Chemical shift difference plot of unbound I-2 versus PSI-bound I-2 indicates that residues in the RVxF motif of I-2 are in similar environments in unbound I-2 and in the PSI complex. Only residues in the SILK motif and the C-terminal helix show significant differences in chemical shifts. (D) Chemical shift difference plot of PSI-bound I-2 versus PI-bound I-2 indicates that residues in the SILK motif and the C-terminal helix of I-2 are in similar environments in PSI and PI complexes. Only residues in the RVxF motif show significant changes in chemical shifts between these two complexes. This indicates that the I-2 RVxF motif releases from PP1 during the formation of PSI. (E) Pull-down assays (error bars are based on three independent measurements performed in triplicate) of I-2 mutants using PP1-bound Ni-NTA resin (black bars) or PS-bound Ni-NTA resin (gray bars). The SILK mutant is I13A/L14A/K15A, the RVxF mutant 1 is W46A, the RVxF mutant 2 is K42A/Q44G, and the helix mutant is R157A/D163A. Binding to PP1 alone is affected equally by mutations in all three regions of I-2 that interact with PP1. However, mutation of the SILK motif has a dramatic affect on the binding of I-2 to PSI, indicating its increased importance after release of the I-2 RVxF motif from PP1.

NMR Spectroscopy of PS and PSI. To determine if a structural rearrangement of spinophilin plays a role in the formation of PSI, we undertook NMR spectroscopy studies of spinophilin in the PS and PSI complexes. We previously completed the sequence-specific backbone assignment of unbound spinophilin, which was used for the analysis of the PS and PSI spectra (*9*, *37*, *38*). The overlay of the 2D [^{1}H,^{15}N]-HSQC/TROSY spectra of unbound ^{15}N-labeled spinophilin and ^{2}H,^{15}N-labeled spinophilin in the PS complex is shown in Figure 3A, while the overlay of the 2D [^{1}H,^{15}N]-TROSY spectra of ^{2}H,^{15}N-labeled spinophilin in the PS and PSI complexes is shown in Figure 3B. Unbound spinophilin shows limited preference for transient secondary and tertiary structure throughout its PP1 binding domain (*12*). However, upon binding to PP1, secondary structure elements are formed in the PP1 binding domain, following restriction to a single conformation (*9*). As is expected for such a significant folding-upon-binding transition, the 2D [^{1}H,^{15}N]-HSQC/TROSY spectra of unbound spinophilin and spinophilin in the PS complex are significantly different. Therefore, it was not possible to transfer the assignment of unbound spinophilin onto PP1-bound spinophilin. Due to the low stability of the complex (~20 h, 120 μM) it was impossible to record the necessary 3D NMR spectra in a quality that would allow for the sequence-specific backbone assignment determination of spinophilin in the PS complex. However, ~15 peaks differ in the 2D [^{1}H,^{15}N]-TROSY spectra of spinophilin in the PS and PSI complexes, indicating that the local environment of these spinophilin residues is different in these two complexes, due to I-2 binding.

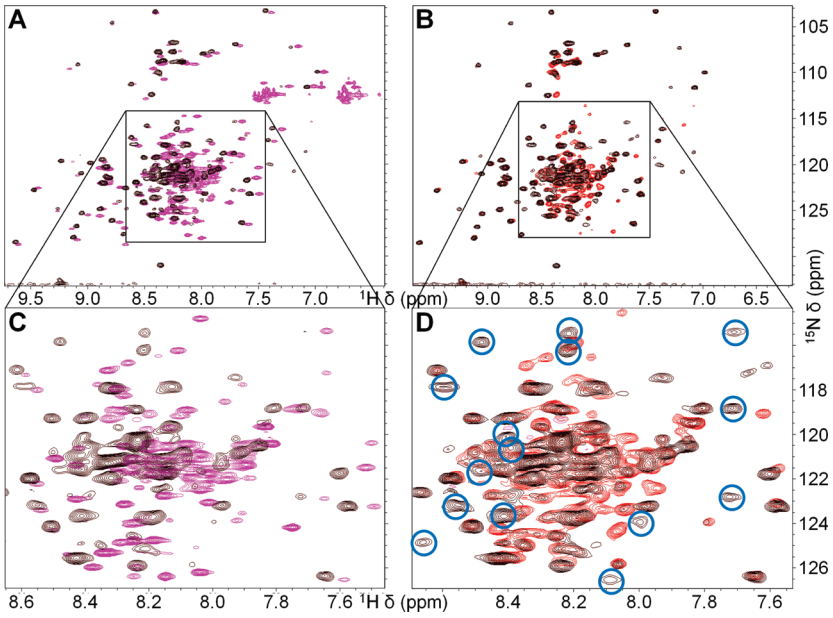

FIGURE 3: Structural rearrangement is seen in spinophilin upon formation of PSI. (A) Overlay of the [^{1}H,^{15}N]-HSQC spectrum of unbound spinophilin (pink) and the [^{1}H,^{15}N]-TROSY spectrum of PPI-bound spinophilin (black). Major changes in spinophilin between the two spectra are due to the folding-upon-binding transition spinophilin undergoes upon binding to PP1. (B) Overlay of the [^{1}H,^{15}N]-TROSY spectra of PPI-bound spinophilin (black) and PSI-bound spinophilin (red). Limited differences between the two spectra indicate that spinophilin does not undergo a large conformational rearrangement between the PS and PSI complexes. However, ~15 residues exhibit significant chemical shift changes (highlighted by blue circles in zoom-in frame D).

Table 2: Statistics for SAXS Analysis of the PSI Complex[a]

	PSI
Guinier approximation	
R_g (Å)	37.1 ± 1.0
$P(r)$ function calculation	
q-range (Å^{-1})	0.015−0.300
R_g (Å)	36.5
D_{max} (Å)	125
structure modeling	
χ	1.30 ± 0.03
NSD[a]	1.37 ± 0.04
NSD[m]	2.02

[a]NSD[a] is the discrepancy between the *ab initio* models. NSD[m] is the discrepancy between the envelope and the PS and PI overlay model.

SAXS Analysis of the Heterotrimeric PSI Complex. To gain further structural insights into the heterotrimeric PSI complex, we performed small angle X-ray scattering (SAXS), which reports on the overall size and shape of a protein in solution (Supporting Information Figure S3, Table 2). SAXS data were recorded at multiple concentrations, and Guinier analysis of the PSI complex reported a radius of gyration of 37.1 ± 1.0 Å (Figure 4A). For the initial analysis of the SAXS data we created a PSI model (thereafter referred to as PSIm) based on a superposition of the PS X-ray crystal structure and the PI ensemble structure (*12*). Interestingly, the calculated R_g of the PSIm structure is only 33.7 Å and thus significantly smaller than the experimental value based on the Guinier approximation. This shows that the PSIm superposition model does not provide a good representation of the PSI complex, and the formation of PSI results in a more extended structure.

Next, GASBOR was used to calculate an *ab initio* molecular envelope of the PSI complex (Figure 4B) (*30*). Sixteen independent *ab initio* models were created with a maximal length of 125 Å as determined by the analysis of the pair−distance distribution function (Supporting Information Figure S3C). The *ab initio* models were then averaged and the models aligned with a normalized spatial discrepancy (NSD[a]) of 1.37 ± 0.04 (*32*). The alignment of the PSI envelope with PSIm resulted in a poor NSD[m] of 2.02. Interestingly, the *ab initio* envelope contains additional density that does not directly correlate with any structural elements of PSIm. These results further support our NMR and biochemical data which show that both spinophilin and I-2 exhibit increased flexibility due to the structural rearrangements that accompany PSI complex formation. Therefore, PSI cannot be accurately described by a single structure.

Ensemble Model for PSI. To further refine the conformation of the PSI complex in solution, we used the program BILBOMD (*33*), which samples conformational space using molecular dynamics (MD) simulations and subsequently selects for the models that have the best agreement between the theoretical and experimental scattering data. The PSIm superposition model and information from the NMR spectroscopy and biochemistry experiments were used to define regions of rigidity and flexibility. The NMR analysis of I-2 in the PSI complex shows that the chemical shifts of the I-2 C-terminal helix in the PI and PSI complexes are identical, indicating that the I-2 helix interactions observed in the PI crystal structure are also present in the PSI complex. However, this implies that the position of the spinophilin helix must change upon heterotrimeric PSI complex formation. Thus, PP1 (residues 7−300; electron density in the PP1−spinophilin structure), spinophilin residues 424−476 (electron density in the PP1−spinophilin structure), and the I-2 SILK motif (residues 11−16; electron density in the PP1−I-2 structure) and helix of I-2 (residues 130−164; electron density in the PP1−I-2 structure) were fixed as rigid body 1, which was not allowed to move. The spinophilin PDZ domain (residues 494−583; electron density in the PP1−spinophilin structure) was defined as rigid body 2, which was allowed to move relative to rigid body 1. Based on our NMR data, spinophilin residues 477−493 (helix) and I-2 residues 9−10 (N-terminal

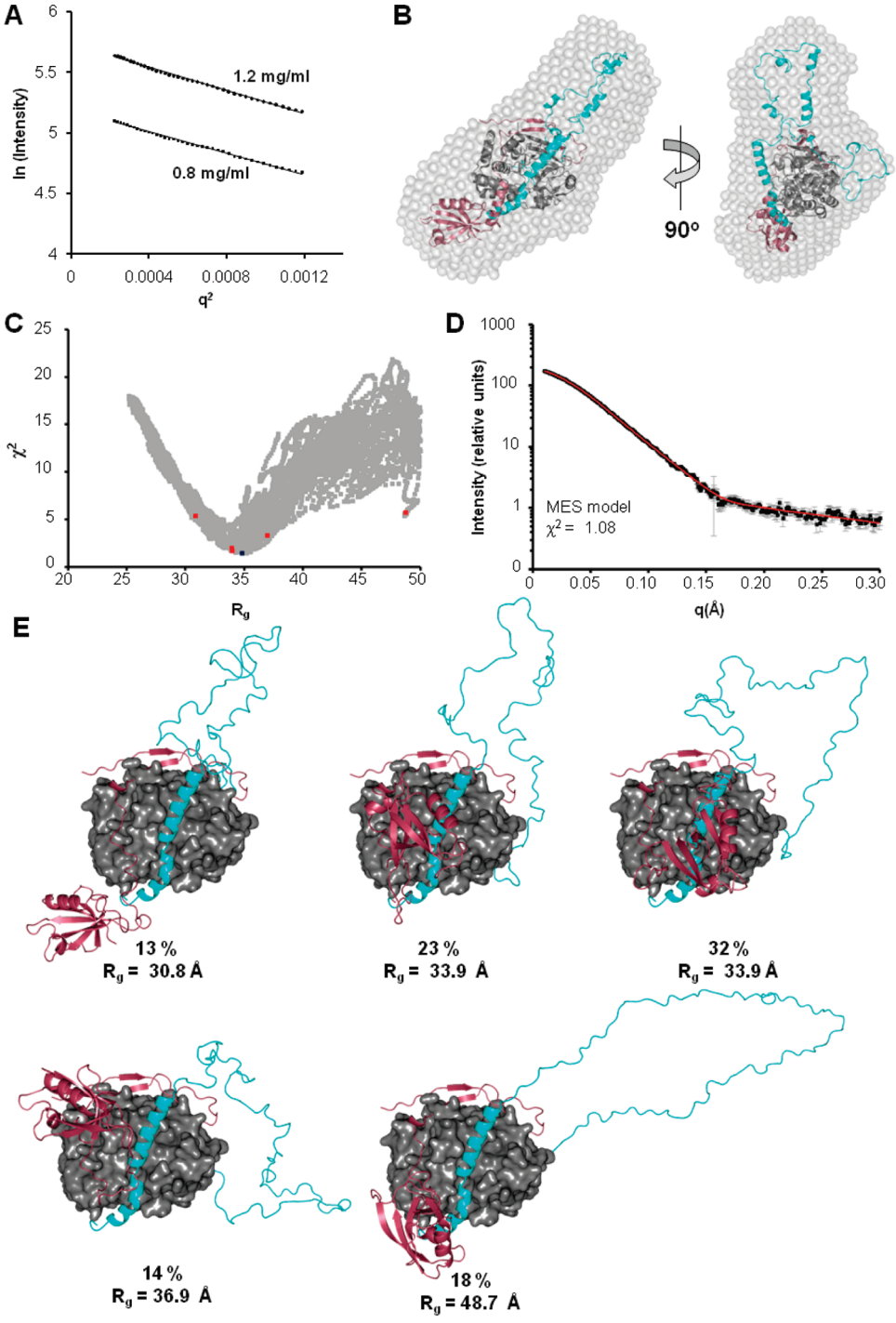

FIGURE 4: SAXS analysis of the PSI complex. (A) The Guinier region of the scattering curve for data recorded at 0.8 and 1.2 mg/mL. (B) *Ab initio* envelope for PSI. Overlay of the *ab initio* envelope (gray surface representation) with the PS crystal structure and one structure from the PI ensemble model. All structures are shown as cartoon images with spinophilin in red, PP1 in black, and I-2 in cyan. BILBOMD analysis of the PSI complex was carried out. (C) Graph comparing the R_g to the χ^2 for the 12000 structures generated during MD simulations (gray squares). χ^2 is the discrepancy between the theoretical scattering and the experimental data. The data point corresponding to the single best fit structure is shown blue, and the data points for the five structures of the MES model are shown in red. (D) Comparison of the theoretical scattering data (red line) for the best fit MES model to the experimental scattering data (black squares). (E) The five structures of the MES model are shown with PP1 in gray as a surface representation and spinophilin and I-2 as cartoon representations in red and cyan, respectively. The relative percent populations are listed below each structure along with the R_g for each structure.

to the SILK motif) and I-2 residues 17−129 were defined as flexible.

As expected, the generated PSI structures sample a broad conformational space with an R_g between 25.1 and 50.0 Å. Theoretical scattering data from a single best fit structure fits the data with a χ^2 = 1.47. A minimal ensemble search (MES) model of five structures provides a better fit to the experimental data with a χ^2 = 1.08 (Figure 4C,D). Individually, each structure of the ensemble has a significantly worse fit to the data, demonstrating that the structure of the PSI complex can only be described as an ensemble of structures. The five ensemble structures that form the PSI MES include an R_g range from 30.8 to 48.7 Å and are represented from 13% to 32% (Figure 4E). These structures

provide an insight into the increased flexibility of I-2 and spinophilin in the PSI complex.

DISCUSSION

Recently, it was shown that pairs of PP1 targeting and inhibitor proteins can interact with PP1 simultaneously to form heterotrimeric holoenzymes (*13*−*15*). However, until now, no detailed biochemical and structural information for any PP1−targeting protein−inhibitor protein triple complex has ever been reported. By integrating the results from NMR spectroscopy, biochemistry, ICP-AES, and SAXS, we now show that major structural rearrangements in both spinophilin (targeting) and inhibitor 2 (I-2, inhibitor), but not in PP1, are essential for the formation of the heterotrimeric PP1−spinophilin−I-2 (PSI) complex. Specifically, our ICP-AES results show that, in the PSI complex, the active site of PP1 is unchanged, with all three complexes (PS, PI, and PSI) containing two Mn^{2+} ions. In contrast, our NMR, biochemical, and SAXS data show that the PP1 regulatory proteins undergo significant structural rearrangements upon PSI complex formation, with the RVxF motif of spinophilin displacing that of I-2 and the helix of I-2 displacing that of spinophilin, leading to an increase in the flexibility of both PP1 regulatory proteins. Furthermore, due to this increased flexibility, the PSI structure cannot be described as a single conformer but instead must be described as an ensemble of structures. Collectively, these data provide the first insights into the molecular interactions that enable PP1 heterotrimeric complexes to exploit the targeting and inhibitory characteristics of PP1 regulatory proteins to form multifunctional PP1 holoenzymes.

Because of its vital importance for PP1 binding, numerous bioinformatics and biochemical analysis of the amino acid composition of the RVxF motif have been described (*5*, *6*, *23*, *39*). For instance, a biochemical RVxF motif analysis identified that mGluR7b with K, H, and F in RVxF motif positions 2, 4, and 5, respectively, pulled down more PP1 than S, K, and W in these same positions (*39*). This predicts that the RVxF motif of spinophilin ($RKIHF^{447-451}$) interacts more tightly with PP1 than that of I-2 ($KSQKW^{42-46}$). In line with this, our NMR spectroscopy data show that the RVxF motif of I-2 is released from PP1 upon formation of PSI, while the RVxF motif of spinophilin remains bound to PP1. The same will likely hold true for other heterotrimeric PP1 complexes, indicating that it may be possible to predict which regulatory protein releases from the RVxF binding site based on the RVxF sequences. Release of the RVxF motif of I-2 from PP1 increases the importance of the SILK motif in the formation of PSI. I-2 is one of the most ancient PP1 regulatory proteins, and the SILK motif is highly conserved among opisthokonts and amoebozoa (*40*). Therefore, it is predicted that SILK motifs are present in other PP1 regulatory proteins. So far, seven additional PP1 regulators have been identified with a SILK or SILK-like motif (*5*). Critically, these studies show the SILK motif is an essential motif for anchoring regulatory proteins to PP1, especially when other binding motifs, such as the RVxF motif, are released or displaced. Additionally, our mutagenesis data have also revealed the importance of residues forming electrostatic interactions between the helix of I-2 and PP1 for binding. As we have previously shown, mutations of similar residues on spinophilin had no effect for the ability of spinophilin to bind PP1 (*9*). This clearly lends further support to our model in which I-2 displaces the helix of spinophilin during formation of the PSI complex.

Our NMR and biochemical data show that the PSI complex is highly dynamic. Using SAXS (1000's of crystallization trials of the PSI complex were unsuccessful), we generated an MES model for the PSI complex, which provides the first insights into the overall shape of the complex, including the influence of dynamics on the flexible segments of I-2 and spinophilin. The MES model contains five structures, each represented at similar populations but with varying R_gs. The release of the RVxF motif of I-2 and helix of spinophilin creates a heterotrimeric complex that contains enhanced flexibility compared to the already dynamic heterodimeric complexes. While it is currently unclear what role this enhanced flexibility has, a possibility is that it could alter the function of both spinophilin and I-2. For example, the enhanced flexibility of the heterotrimeric complex creates a more extended and flexible PDZ domain of spinophilin than in PS. This could allow the PDZ domain to bind its targets more efficiently, or create a larger substrate capture radius, in a model similar to the proposed "fly casting" mechanism (*41*). Similarly, the more extended nature of I-2 could also create new protein interaction sites which were previously buried in the PI complex. Thus by forming the heterotrimeric PSI complex, the best of both "PP1 worlds" is optimally combined: 1) PP1 targeting is mediated by the multidomain protein spinophilin and 2) PP1 inhibition is mediated by I-2, although I-2 most likely does not activate PP1 until "triggered" by outside inputs such as phosphorylation of Thr-72 on I-2.

ACKNOWLEDGMENT

The authors thank Dr. Lin Yang (NSLS) for support at beamline X9, Dr. Michal Hammel (LBL) for help with BILBOMD, and Dr. David Murray and Mr. Joseph Orchardo (Brown University Center for Environmental Studies Core Facilities) for access and help with the ICP-AES measurements.

SUPPORTING INFORMATION AVAILABLE

Figures S1−S3 showing an overlay of the PP1−spinophilin and PP1−I-2 crystal structures, CD spectra of all I-2 mutants, and SAXS data for the PSI complex and Table S1 showing the Michaelis−Menten constants measured for different PP1 complexes. This material is available free of charge via the Internet at http://pubs.acs.org.

REFERENCES

1. Cohen, P. T. (2002) Protein phosphatase 1—targeted in many directions. *J. Cell Sci. 115*, 241–256.
2. Ceulemans, H., and Bollen, M. (2004) Functional diversity of protein phosphatase-1, a cellular economizer and reset button. *Physiol. Rev. 84*, 1–39.
3. Barford, D. (1996) Molecular mechanisms of the protein serine/threonine phosphatases. *Trends Biochem. Sci. 21*, 407–412.
4. Goldberg, J., Huang, H. B., Kwon, Y. G., Greengard, P., Nairn, A. C., and Kuriyan, J. (1995) Three-dimensional structure of the catalytic subunit of protein serine/threonine phosphatase-1. *Nature 376*, 745–753.
5. Bollen, M., Peti, W., Ragusa, M. J., and Beullens, M. (2010) The extended PP1 toolkit: designed to create specificity. *Trends Biochem. Sci. 35*, 450–458.
6. Hendrickx, A., Beullens, M., Ceulemans, H., Abt, T. D., Van Eynde, A., Nicolaescu, E., Lesage, B., and Bollen, M. (2009) Docking motif-guided mapping of the interactome of protein phosphatase-1. *Chem. Biol. 16*, 365–371.
7. Aggen, J. B., Nairn, A. C., and Chamberlin, R. (2000) Regulation of protein phosphatase-1. *Chem. Biol. 7*, R13–23.
8. Bollen, M. (2001) Combinatorial control of protein phosphatase-1. *Trends Biochem. Sci. 26*, 426–431.

9. Ragusa, M. J., Dancheck, B., Critton, D. A., Nairn, A. C., Page, R., and Peti, W. (2010) Spinophilin directs protein phosphatase 1 specificity by blocking substrate binding sites. *Nat. Struct. Mol. Biol. 17*, 459–464.
10. Terrak, M., Kerff, F., Langsetmo, K., Tao, T., and Dominguez, R. (2004) Structural basis of protein phosphatase 1 regulation. *Nature 429*, 780–784.
11. Hurley, T. D., Yang, J., Zhang, L., Goodwin, K. D., Zou, Q., Cortese, M., Dunker, A. K., and DePaoli-Roach, A. A. (2007) Structural basis for regulation of protein phosphatase 1 by inhibitor-2. *J. Biol. Chem. 282*, 28874–28883.
12. Marsh, J. A., Dancheck, B., Ragusa, M. J., Allaire, M., Forman-Kay, J. D., and Peti, W. (2010) Structural diversity in free and bound states of intrinsically disordered protein phosphatase 1 regulators. *Structure 18*, 1094–1103.
13. Terry-Lorenzo, R. T., Elliot, E., Weiser, D. C., Prickett, T. D., Brautigan, D. L., and Shenolikar, S. (2002) Neurabins recruit protein phosphatase-1 and inhibitor-2 to the actin cytoskeleton. *J. Biol. Chem. 277*, 46535–46543.
14. Connor, J. H., Weiser, D. C., Li, S., Hallenbeck, J. M., and Shenolikar, S. (2001) Growth arrest and DNA damage-inducible protein GADD34 assembles a novel signaling complex containing protein phosphatase 1 and inhibitor 1. *Mol. Cell. Biol. 21*, 6841–6850.
15. Lesage, B., Beullens, M., Pedelini, L., Garcia-Gimeno, M. A., Waelkens, E., Sanz, P., and Bollen, M. (2007) A complex of catalytically inactive protein phosphatase-1 sandwiched between Sds22 and inhibitor-3. *Biochemistry 46*, 8909–8919.
16. Allen, P. B., Ouimet, C. C., and Greengard, P. (1997) Spinophilin, a novel protein phosphatase 1 binding protein localized to dendritic spines. *Proc. Natl. Acad. Sci. U.S.A. 94*, 9956–9961.
17. Feng, J., Yan, Z., Ferreira, A., Tomizawa, K., Liauw, J. A., Zhuo, M., Allen, P. B., Ouimet, C. C., and Greengard, P. (2000) Spinophilin regulates the formation and function of dendritic spines. *Proc. Natl. Acad. Sci. U.S.A. 97*, 9287–9292.
18. Greengard, P. (2001) The neurobiology of slow synaptic transmission. *Science 294*, 1024–1030.
19. Oliver, C. J., and Shenolikar, S. (1998) Physiologic importance of protein phosphatase inhibitors. *Front. Biosci. 3*, D961–D972.
20. Kakinoki, Y., Somers, J., and Brautigan, D. L. (1997) Multisite phosphorylation and the nuclear localization of phosphatase inhibitor 2-green fluorescent protein fusion protein during S phase of the cell growth cycle. *J. Biol. Chem. 272*, 32308–32314.
21. Brautigan, D. L., Sunwoo, J., Labbe, J. C., Fernandez, A., and Lamb, N. J. (1990) Cell cycle oscillation of phosphatase inhibitor-2 in rat fibroblasts coincident with p34cdc2 restriction. *Nature 344*, 74–78.
22. Senba, S., Eto, M., and Yazawa, M. (1999) Identification of trimeric myosin phosphatase (PP1M) as a target for a novel PKC-potentiated protein phosphatase-1 inhibitory protein (CPI17) in porcine aorta smooth muscle. *J. Biochem. 125*, 354–362.
23. Egloff, M. P., Johnson, D. F., Moorhead, G., Cohen, P. T., Cohen, P., and Barford, D. (1997) Structural basis for the recognition of regulatory subunits by the catalytic subunit of protein phosphatase 1. *EMBO J. 16*, 1876–1887.
24. Kelker, M. S., Page, R., and Peti, W. (2009) Crystal structures of protein phosphatase-1 bound to nodularin-R and tautomycin: a novel scaffold for structure-based drug design of serine/threonine phosphatase inhibitors. *J. Mol. Biol. 385*, 11–21.
25. Dancheck, B., Nairn, A. C., and Peti, W. (2008) Detailed structural characterization of unbound protein phosphatase 1 inhibitors. *Biochemistry 47*, 12346–12356.
26. Konarev, P. V., Volkov, V. V., Sokolova, A. V., Koch, M. H. J., and Svergun, D. I. (2003) PRIMUS: a Windows PC-based system for small-angle scattering data analysis. *J. Appl. Crystallogr. 36*, 1277–1282.
27. Guinier, A. (1939) La diffraction des rayons X aus tres petits angles: application a l'etude de phenomenes ultramicroscopiques. *Ann. Phys. 12*, 161–237.
28. de la Torre, J. G., Huertas, M. L., and Carrasco, B. (2000) Calculation of hydrodynamic properties of globular proteins from their atomic-level structure. *Biophys. J. 78*, 719–730.
29. Svergun, D. I. (1992) Determination of the regularization parameter in indirect transform methods using perceptual criteria. *J. Appl. Crystallogr. 26*, 495–503.
30. Svergun, D. I., Petoukhov, M. V., and Koch, M. H. J. (2001) Determination of domain structure of proteins from X-ray solution scattering. *Biophys. J. 80*, 2946–2953.
31. Volkov, V. V., and Svergun, D. I. (2003) Uniqueness of ab initio shape determination in small-angle scattering. *J. Appl. Crystallogr. 36*, 860–864.
32. Kozin, M. B., and Svergun, D. I. (2001) Automated matching of high- and low-resolution structural models. *J. Appl. Crystallogr. 34*, 33–41.
33. Pelikan, M., Hura, G. L., and Hammel, M. (2009) Structure and flexibility within proteins as identified through small angle X-ray scattering. *Gen. Physiol. Biophys. 28*, 174–189.
34. Schneidman-Duhovny, D., Hammel, M., Sali, A. (2010) FoXS: a web server for rapid computation and fitting of SAXS profiles, *Nucleic Acids Res.*
35. Huang, H. B., Horiuchi, A., Watanabe, T., Shih, S. R., Tsay, H. J., Li, H. C., Greengard, P., and Nairn, A. C. (1999) Characterization of the inhibition of protein phosphatase-1 by DARPP-32 and inhibitor-2. *J. Biol. Chem. 274*, 7870–7878.
36. Connor, J. H., Frederick, D., Huang, H., Yang, J., Helps, N. R., Cohen, P. T., Nairn, A. C., DePaoli-Roach, A., Tatchell, K., and Shenolikar, S. (2000) Cellular mechanisms regulating protein phosphatase-1. A key functional interaction between inhibitor-2 and the type 1 protein phosphatase catalytic subunit. *J. Biol. Chem. 275*, 18670–18675.
37. Kelker, M. S., Dancheck, B., Ju, T., Kessler, R. P., Hudak, J., Nairn, A. C., and Peti, W. (2007) Structural basis for spinophilin-neurabin receptor interaction. *Biochemistry 46*, 2333–2344.
38. Kelker, M. S., and Peti, W. (2006) NMR assignment of the spinophilin PDZ domain (493−602). *J. Biomol. NMR 36* (Suppl. 1), 24.
39. Meiselbach, H., Sticht, H., and Enz, R. (2006) Structural analysis of the protein phosphatase 1 docking motif: molecular description of binding specificities identifies interacting proteins. *Chem. Biol. 13*, 49–59.
40. Ceulemans, H., Stalmans, W., and Bollen, M. (2002) Regulator-driven functional diversification of protein phosphatase-1 in eukaryotic evolution. *BioEssays 24*, 371–381.
41. Shoemaker, B. A., Portman, J. J., and Wolynes, P. G. (2000) Speeding molecular recognition by using the folding funnel: the fly-casting mechanism. *Proc. Natl. Acad. Sci. U.S.A. 97*, 8868–8873.